JOURNAL OF VIROLOGY, Mar. 2010, p. 2522–2532 Vol. 84, No. 5
0022-538X/10/$12.00 doi:10.1128/JVI.01883-09

Sequestration of Free Tubulin Molecules by the Viral Protein NSP2 Induces Microtubule Depolymerization during Rotavirus Infection▽§

Davy Martin,[1]* Mariela Duarte,[1,2] Jean Lepault,[1] and Didier Poncet[1]*

Virologie Moléculaire et Structurale, CNRS UMR 2472, INRA UMR 1157, IFR 115, Avenue de la Terrasse, 91198 Gif sur Yvette, France,[1] and Université d'Evry Val d'Essonne, 91025 Evry, France[2]

Received 4 September 2009/Accepted 11 December 2009

Microtubules, components of the cell cytoskeleton, play a central role in cellular trafficking. Here we show that rotavirus infection leads to a remodeling of the microtubule network together with the formation of tubulin granules. While most microtubules surrounding the nucleus depolymerize, others appear packed at the cell periphery. In microtubule depolymerization areas, tubulin granules are observed; they colocalize with viroplasms, viral compartments formed by interactions between rotavirus proteins NSP2 and NSP5. With purified proteins, we show that tubulin directly interacts *in vitro* with NSP2 but not with NSP5. The binding of NSP2 to tubulin is independent of its phosphatase activity. The comparison of three-dimensional (3-D) reconstructions of NSP2 octamers alone or associated with tubulin reveals electron densities in the positively charged grooves of NSP2 that we attribute to tubulin. Site-directed mutagenesis of NSP2 and competition assays between RNA and tubulin for NSP2 binding confirm that tubulin binds to these charged grooves of NSP2. Although the tubulin position within NSP2 grooves cannot be precisely determined, the tubulin C-terminal H12 α-helix could be involved in the interaction. NSP2 overexpression and rotavirus infection produce similar effects on the microtubule network. NSP2 depolymerizes microtubules and leads to tubulin granule formation. Our results demonstrate that tubulin is a viroplasm component and reveal an original mechanism. Tubulin sequestration by NSP2 induces microtubule depolymerization. This depolymerization probably reroutes the cell machinery by inhibiting trafficking and functions potentially involved in defenses to viral infections.

Microtubules (MTs) are components of the cell cytoskeleton and play a major role in cellular trafficking. Molecular motors (dynein and kinesins) use MTs as tracks to address organelles to precise loci. Viruses are irreplaceable tools to study cellular processes; for example, many of them hijack cellular transport to reach the perinuclear region (for reviews, see references 27, 35, 39, and 40). Some viruses also modify the cell compartmentation and create viral inclusions where viral replication and virion assembly are performed (for a review, see reference 30). Both aspects are sometimes related; electron and fluorescence microscopy observations of reovirus-infected cells have shown that viral inclusions form an electron-dense coat surrounding the MTs (15, 32, 41). In the case of rotavirus, another member of the *Reoviridae* family, interactions between viral proteins and MTs remain unclear; some studies report an interaction between MTs and either NSP4 or VP4, whereas others did not detect these interactions (4, 19, 29, 51). Rotavirus is the leading agent of gastroenteritis in young children worldwide (31); studying its interactions with its host cell is thus of particular interest to identify new potential therapeutical targets.

The rotavirus genome is composed of 11 double-stranded RNAs (dsRNA) surrounded by a triple-layer capsid. During rotavirus infection, punctuate cytoplasmic structures, named "viroplasms," are formed; they are the sites of viral genome replication and virion assembly. These structures are made of several viral proteins and of viral mRNAs that serve as templates for genome replication. Two viral nonstructural proteins, NSP2 and NSP5, are crucial for viroplasm formation (10, 24, 38). Their coexpression in uninfected cells leads to the formation of punctuate cytoplasmic structures termed viroplasm-like structures (VLS) (18). NSP2 forms a doughnut-shaped octamer by tail-to-tail interaction of two tetramers; four positively charged grooves crossing the two tetramers have been identified (21). Structural and biochemical studies have revealed a histidine-triad (HIT)-like motif responsible for the nucleoside triphosphatase (NTPase), RNA triphosphatase (RTPase), and nucleoside diphosphate (NDP) kinase-like activities of NSP2 (21, 23, 42, 46). These catalytic activities are required for dsRNA synthesis but not for viroplasm formation (11, 43). NSP2 binds single-stranded RNA nonspecifically, has helix destabilizing activity (44), and undertakes conformational changes upon nucleotide binding (37). NSP2 might thus function as a molecular motor involved in genome replication and packaging. NSP5 is a dimeric O-linked glyco- and phosphoprotein, which exists as variously phosphorylated isoforms (1, 36, 48). A cryoelectron microscopy study pointed out that RNA and NSP5 compete for binding to the grooves of the NSP2 octamer (22). The function of NSP5 in rotavirus replication and the role of its phosphorylation remain unknown. No cellular partner of these two nonstructural proteins was known, until a possible association of both proteins with tubulin was reported (9).

In the present report, we studied the interaction of rotavirus with tubulin and MTs. We focused on the cellular effects and

* Corresponding author. Mailing address: Virologie Moléculaire et Structurale, CNRS UMR 2472, INRA UMR 1157, IFR 115, Avenue de la Terrasse, 91198 Gif sur Yvette, France. Phone for Didier Poncet: 33 1 69 82 38 35. Fax: 33 1 69 82 43 08. E-mail: didier.poncet@vms.cnrs-gif.fr. Phone for Davy Martin: 33 1 69 82 38 56. Fax: 33 1 69 82 43 08. E-mail: davy.martin@vms.cnrs-gif.fr.

§ Supplemental material for this article may be found at http://jvi.asm.org/.

▽ Published ahead of print on 23 December 2009.

the structural characterization of the interaction between tubulin and NSP2. Our results highlight that infection by the rotavirus RF strain disorganizes and depolymerizes the MT network of MA104 cells and that viroplasms colocalize with tubulin granules. Electron microscopy and biochemical experiments demonstrate that tubulin directly binds to the positively charged grooves of NSP2. Moreover, NSP2 overexpression induces MT depolymerization and tubulin granule formation. We thus propose that NSP2 sequesters tubulin in viroplasms during rotavirus infection. This sequestration induces the MT depolymerization observed during rotavirus infection and most probably modifies cellular trafficking.

MATERIALS AND METHODS

Plasmid construction and mutagenesis. The plasmid priboz delta P4 was derived from pBluescript SKII(−) and contains a mutated hepatitis delta virus antigenome ribozyme and a T7 terminator sequence downstream from a NotI and an XmaI (CCCGGG) site. Rotavirus cDNA for RF gene 8 (encoding NSP2; GenBank accession no. Z21640) was amplified by reverse transcription-PCR (RT-PCR) using a 5′ primer that contained a NotI site fused to the T7 polymerase promoter abutted to the 5′ noncoding sequence of gene 8 from the RF strain of rotavirus and a 3′ reverse primer corresponding to the 3′ end noncoding sequence, fused to an AgeI site (…**TGACC**ggt with rotavirus 3′ end in capital bold letters and AgeI site underlined). The PCR product was digested with NotI and AgeI and cloned between priboz delta P4 NotI and XmaI sites. The pIres RF08 delta P4 plasmid was obtained by cloning the NotI-NcoI fragment of pTM1 (17) that contained the T7 promoter fused to the EMCV IRES in place of the NotI-NcoI site of priboz RF08 delta P4.

The same strategy was used to clone RF gene 11 (GenBank AF188126) except that, before the EMCV IRES was added, an NcoI site was placed on the ATG translation initiation codon by site-directed mutagenesis, leading to the mutation of serine 2 into alanine (S2A), and HDV ribozyme was inactivated by deleting the P1 region by site-directed mutagenesis (3). The vector was named pIres RF11 S2A delta P1.

For RF08 cloning, the NSP2 cDNA of the bovine RF strain of rotavirus was amplified by PCR and cloned into either the pET28b+ expression vector (Novagen, Darmstadt, Germany) between the NcoI and BamHI restriction sites or the pQE-60 expression vector (Qiagen, Courtaboeuf, France) between the NcoI and BglII restriction sites. pET28b+ RF08 produces an untagged protein, and pQE-60 RF08 produces a recombinant protein with a C-terminal six-His tag.

Mutation of lysines 37, 38, 58, and 59 and arginines 60 and 68 into glutamine was performed using the QuikChange site-directed mutagenesis kit (Stratagene, Massy, France) on the pET28b+ RF08 vector.

To get pACYC RF11 S2A, RF11 was amplified by RT-PCR and cloned into the pACYCDuet-1 vector (Novagen, Darmstadt, Germany) between the NcoI and XhoI restriction sites; the introduction of an NcoI site at the beginning of the coding sequence of RF11 led to the mutation of serine 2 into alanine. This vector produces an untagged protein.

Production and purification of polyclonal rabbit antibodies (pAb) against protein NSP2 of rotavirus strain RF. Recombinant NSP2 with a C-terminal six-His tag was expressed in *Escherichia coli* M15[pREP4], purified by Ni-NTA affinity chromatography (Qiagen, Courtaboeuf, France) as described in reference 42, and used to obtain polyclonal antibodies raised in SPF rabbits, negative for rotavirus antigens by Western blotting, by routine immunogenic procedures (Eurogentec, Herstal, Belgium). In order to remove unspecific antibodies from the serum (no. 5815), an M15(pREP4) cell lysate was adsorbed on a nitrocellulose membrane and suspended in a tank of chloroform vapors for 15 min, cut, and shaken with the antiserum overnight at 4°C. Immunoglobulins G (IgGs) were then purified on a protein A column (Melon gel purification kit; Pierce, Roquefort, IL).

Protein expression and purification. To produce NSP2 or NSP2 K37Q K38Q K58Q K59Q R60Q R68Q, the *E. coli* BL21(DE3) strain was transformed by either pET28b+ RF08 or pET28b+ RF08 K37Q K38Q K58Q K59Q R60Q R68Q plasmids and expression was carried out overnight at 18°C with 0.1 mM IPTG (isopropyl-β-D-thiogalactopyranoside). Bacteria were lysed by sonication in 20 mM Tris-HCl, pH 8.0, 100 mM NaCl, and 1 mM dithiothreitol (DTT) (buffer A). Proteins were purified on a HiTrap Heparin HP column (GE Healthcare, Orsay, France), followed by cation-exchange chromatography on a HiTrap SP HP column (GE Healthcare, Orsay, France) and size exclusion chromatography on a Superdex 200 10/300 GL column (GE Healthcare, Orsay, France) in buffer A with 480 mM NaCl. Western blot and mass spectrometry analyses were performed to confirm the identity of the purified protein (data not shown). In buffer A with 480 mM NaCl, NSP2 formed octamers, as analyzed by size exclusion chromatography and dynamic light scattering (DLS) using a DynaPro (Protein Solution), and was 70% monodisperse by DLS.

To produce NSP5 S2A, the *E. coli* BL21(DE3) strain was transformed by pACYC RF11 S2A, and expression was carried out overnight at 18°C with 0.1 mM IPTG. Bacteria were lysed by sonication in 20 mM morpholinepropanesulfonic acid (MOPS), pH 7.1, 50 mM NaCl, 1 mM EDTA, and 1 mM DTT (buffer B). After centrifugation, the pellet was solubilized in 20 mM MOPS, pH 7.1, 6 M guanine hydrochloride (GuHCl), and 1 mM DTT and dialyzed against buffer B. Proteins were purified by anion-exchange chromatography on a MonoQ 5/50 GL column (GE Healthcare, Orsay, France), followed by size exclusion chromatography on a Superose 6 10/300 GL column (GE Healthcare, Orsay, France) in buffer B with 500 mM NaCl. Western blotting with a monoclonal antibody and mass spectrometry analyses were performed to confirm the identity of the purified protein (data not shown).

Cell culture, transfection, and viral infection. Monkey kidney cells (MA104) were grown as described in reference 20. BSR-T7/5 cells (a clone of hamster kidney cells [BHK-21] stably expressing the T7 bacteriophage RNA polymerase [7]) were grown at 37°C in a 5% CO_2–air atmosphere in Dulbecco's minimum Eagle's medium (DMEM) (Lonza, Basel, Switzerland) containing 10% fetal bovine serum (FBS), 100 IU/ml of penicillin, 100 μg/ml of streptomycin, and 1 mg/ml of Geneticin (Invitrogen, Cergy Pontoise, France).

The bovine RF strain of group A rotaviruses was used to infect MA104 cells. Infections were performed at a multiplicity of infection (MOI) of 5 PFU/cell in Eagle's minimum essential medium (EMEM) (Lonza, Basel, Switzerland) in the presence of trypsin (0.44 μg/ml type IX trypsin; Sigma, Saint Quentin Fallavier, France) and antibiotics but without serum. Cells were harvested 6 h after infection. Nocodazole (Sigma, Saint Quentin Fallavier, France) treatments were performed at a final concentration of 2 μM in EMEM and at 37°C during the desired time.

Protein expression was carried out by transfecting BSR-T7/5 cells with the pIres vectors and Lipofectamin 2000 (Invitrogen, Cergy Pontoise, France) according to the manufacturer's protocol. Cells were incubated for 1 day at 37°C in a 5% CO_2–air atmosphere in DMEM.

Immunofluorescence microscopy. Samples were prepared as described in reference 20 with the following modifications. In transfection experiments, a 2-min pre-lysis with 0.5% Triton X-100 in PHEM buffer [60 mM PIPES {piperazine-*N*,*N*′-bis(2-ethanesulfonic acid)}, 25 mM HEPES (pH 6.9), 10 mM EGTA, 2 mM $(AcO)_2Mg$] was performed prior to fixation. Cells were fixed in 4% paraformaldehyde (PFA), 0.05% glutaraldehyde, 0.5% Triton X-100 in PHEM buffer for 12 min. Immunostaining was performed with rabbit anti-NSP2 polyclonal antibody (pAb) (1:200) and/or mouse anti-NSP5 monoclonal antibody (MAb) (1:2,000) (36) and was followed by incubations with Alexa Fluor 546 goat anti-rabbit IgG antibody and/or Alexa Fluor 633 goat anti-mouse IgG antibody (Molecular Probes, Inc., Eugene, OR) (1:2,000) and then with mouse monoclonal anti-α-tubulin-fluorescein isothiocyanate (FITC) (Sigma, Saint Quentin Fallavier, France) (1:100). Confocal laser microscopy was performed on a Leica SP2 microscope (63× or 100× magnification oil immersion objectives) using UV argon laser excitation at 451 and 464 nm, blue laser excitation at 488 nm, green laser excitation at 543 nm, and red laser excitation at 633 nm. Data were recorded using a frame sequential mode and narrow wavelength passes to sequentially excite each fluorophore and record its fluorescence frame after frame; the thickness of the sections was 290 nm. Epifluorescence microscopy was performed on a Reichert (POLYVAR) microscope (40× magnification oil immersion objective).

Immunoblot analysis. At 6 h postinfection (MOI of 5 PFU/cell), MA104 cells, either uninfected or rotavirus infected, were recovered in loading buffer (10 mM Tris-HCl, pH 6.8, 2% sodium dodecyl sulfate [SDS], 10% glycerol, 150 mM β-mercaptoethanol). Immunoblotting was performed as described in reference 20 with a mouse anti-α-tubulin MAb (Sigma, Saint Quentin Fallavier, France) (1:1,000) and a mouse anti-glyceraldehyde-3-phosphate dehydrogenase (GAPDH) MAb (Abcam, Cambridge, United Kingdom) (1:10,000). Bands on films were quantified using an ImageScanner and the ImageQuant TL software (GE Healthcare, Orsay, France).

Flow cytometry. Cells were washed with EMEM and then incubated for 5 min with 0.2% (wt/vol) trypsin and 1 mM EDTA in phosphate-buffered saline (PBS) at 37°C. EMEM containing 10% FBS was added to the cells. Cells were centrifuged 5 min at 1,000 × *g*, washed with 4% bovine serum albumin in PHEM buffer, and centrifuged again. Cells were fixed with 4% PFA and 0.5% Triton X-100 in PHEM buffer for 20 min and centrifuged. Cells were then incubated in

PBS-TB (4% boiled horse serum, 0.1% Triton X-100 in PBS) for 25 min and centrifuged. Cells were immunostained with mouse anti-α-tubulin MAb-FITC (1:100) in PBS-TB for 1 h, centrifuged, washed with PBS-TB, and centrifuged again. Cells were resuspended in PBS and analyzed on an EPICS ELITE ESP cytometer (Beckman-Coulter) using argon laser excitation at 488 nm and a 525/30 nm emission filter. For each run, 10,000 cells were analyzed. Data are means ± standard errors of the means of results from four independent experiments. Differences between means were evaluated by paired *t* test, with $P < 0.05$ being taken as the level of significance.

Pull-down and competition assay using NSP2- or NSP5 S2A- or tubulin-cross-linked Sepharose beads. NSP2 or NSP5 S2A or sheep brain tubulin (a gift from M. Knossow, LEBS, Gif/Yvette, France) were coupled with Sepharose beads using *N*-hydroxysuccinimide (NHS)-activated Sepharose 4 Fast Flow (GE Healthcare, Orsay, France) according to the manufacturer's protocol. A 10-μl portion of either uncoupled Sepharose beads or coupled Sepharose beads was mixed with 10 μg of purified potential partner in 100 μl of buffer C (20 mM Na_2HPO_4/NaH_2PO_4, pH 7.2, 150 mM NaCl, 0.5 mM EDTA, 0.5 mM DTT) at 4°C for 1 h. Beads were collected by centrifugation at 500 × *g* for 5 min, and flowthroughs were kept for SDS-PAGE analysis. Beads were washed three times with buffer C. Then, 10 μl of SDS sample buffer was added to the beads for SDS-PAGE analysis. Coomassie blue-stained bands were quantified using an ImageScanner and the ImageQuant TL software.

For competition assays, 10 μl of tubulin-coupled Sepharose beads was mixed with 1 μM NSP2 in 100 μl of buffer C at 4°C for 30 min; then, RNA (*Saccharomyces cerevisiae* tRNA reference 83853; Sigma, Saint Quentin Fallavier, France) was added at different concentrations and the mixtures were incubated for 30 min. Alternatively, RNA and NSP2 were first incubated together and then added to tubulin-coupled Sepharose beads. Beads were collected, washed, and analyzed as reported above.

Microtubule polymerization. A 5-mg/ml sheep tubulin solution in 80 mM PIPES, pH 6.8, 2 mM $MgCl_2$, 1 mM EGTA, 1 mM GTP was polymerized at 37°C for 1 h by the addition of 8% DMSO. Microtubules (MTs) were stabilized by the addition of 1 mM paclitaxel (Sigma, Saint Quentin Fallavier, France) and left overnight at room temperature. MTs were then pelleted for 30 min at 200,000 × *g* and resuspended at 4 μM in 20 mM HEPES, pH 7.2, 150 mM NaCl, 1 mM DTT, 1 mM EGTA, 1 mM $MgCl_2$, 200 μM GTP, 200 μM paclitaxel, 2% DMSO.

Electron microscopy. Three microliters of purified NSP2 octamers incubated or not with dimeric tubulin (molar ratio, 1:4) in 20 mM HEPES, pH 7.2, 150 mM NaCl, 1 mM DTT, 1 mM EGTA, and 1 mM $MgCl_2$ was deposited on air glow-discharged carbon-coated grids. The excess solution was removed with a filter paper, and samples were negatively stained with 2% uranyl acetate or phosphotungstic acid (pH 6.0) solutions. Observations were performed with a Philips CM12 electron microscope operated at 80 kV. Micrographs were recorded at a magnification of 35,000 on SO163 image film (Kodak, Paris, France) developed for 5 min in full-strength D19. A similar treatment was carried out to image paclitaxel-stabilized MTs incubated with or without 0.05 μM NSP2.

For image analysis, the quality of micrographs was checked by optical diffraction. Suitable micrographs were digitized using a Nikon Coolscan 8000 with a raster size of 12.7 μm corresponding to 0.363 nm at the object level. Particles were selected with the ×3d program (14). Individual images were corrected for the phase contrast effects using the ctfit program (26). Electron microscopy reconstruction was performed with the Imagic software (45) imposing D4 (4-2-2) symmetry. The final reconstruction was calculated with 562 particle images (4,496 NSP2 monomers) selected on two negatives that were underfocused by 1.2 and 1.4 μm. The reconstruction of NSP2 in complex with tubulin was performed using the previous NSP2 reconstruction as the initial reference model. Particles were selected on four negatives underfocused by 0.9, 1.2, 1.4, and 1.5 μm. The final reconstruction was calculated with 394 particle images (3,152 NSP2 monomers). The resolutions of the reconstructions were estimated by Fourier shell correlation to 2.5 nm in both cases, using the 0.5 correlation criteria. The difference between the NSP2-tubulin and NSP2 maps was calculated with Imagic. Figures of the maps were rendered using the program PyMOL (http://www.pymol.org).

The SA11 NSP2 atomic model (accession no. 1L9V in the Protein Data Bank) was fitted in our reconstruction using the UROX software (X. Siebert and J. Navaza, unpublished program), which stemmed from the URO program (28). The fit was performed in reciprocal space taking into account the symmetry of the reconstruction. This allows the whole electron microscopy (EM) map to be used without applying a mask around individual molecules in the EM map, as it is often the case in real-space refinement procedures. The quality of the fit was evaluated by calculating correlation coefficients and R factors. They were close to 0.8 and 0.5, respectively, when Fourier coefficients of up to 1/2.5 nm were included. They respectively decreased and increased when higher Fourier coefficients were included, suggesting that the NSP2 map resolution was indeed close to 2.5 nm. The tubulin dimer in the difference map between NSP2-tubulin and NSP2 maps was manually fitted in the difference map using PyMOL.

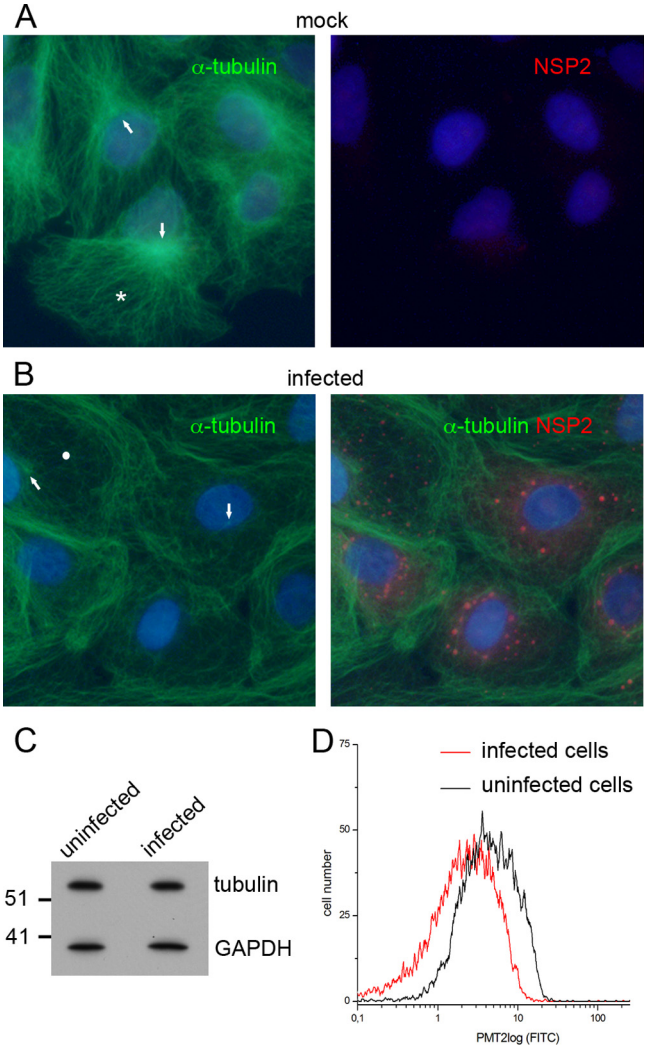

FIG. 1. Rotavirus infection induces modifications in the MT network. (A and B) MA104 cells were either mock infected (A) or infected by rotavirus at an MOI of 5 (B) and then fixed at 6 h postinfection with PFA. Cells were immunostained with rabbit anti-NSP2 pAb and then with Alexa Fluor 546-conjugated goat anti-rabbit IgG (red) together with FITC-conjugated mouse anti-α-tubulin MAb (green). Nuclei were stained with DAPI (blue). Cells were imaged using an epifluorescence microscope. White arrows point at the centrosomes of some cells, and a white star identifies a particular cell. (C) Western blot analysis of the quantity of tubulin inside mock- or rotavirus-infected cells at 6 h postinfection, using GAPDH as a loading control. (D) Flow cytometry analysis of the quantity of MTs inside mock- or rotavirus-infected cells at 6 h postinfection.

RESULTS

Rotavirus infection induces MT depolymerization. To investigate the effects of rotavirus infection on the MT network, we immunostained tubulin in either mock- or rotavirus-infected MA104 cells (Fig. 1A). In uninfected cells, we observed an intense green fluorescence throughout the cytoplasm, reflecting a high MT concentration. The centrosome, from which

MTs irradiate, and its surrounding region had bright staining (indicated in a few cells by a white arrow, Fig. 1A, left panel). The anti-NSP2 antibody gave a very low background (Fig. 1A, right panel). In rotavirus-infected cells, NSP2 expression and viroplasm formation were clearly visible (Fig. 1B, right panel). In those cells, the centrosome was much less bright than in uninfected cells, sometimes barely noticeable (Fig. 1B, left panel), and the MT network appeared less dense than in mock-infected cells. Indeed, MTs were mostly depolymerized around the nucleus of infected cells and closely packed at the cell periphery. Quantitative fluorescence analysis throughout cells (see Fig. S1 in the supplemental material) confirmed that MT distribution was indeed impaired by rotavirus infection and that the MT concentration was lower in infected cells that in uninfected cells. These data clearly show that rotavirus infection disorganizes and damages the MT network.

The decreased amount of MTs in infected cells could result from a reduced quantity of tubulin or MT depolymerization. To discriminate between these two possibilities, Western blotting and flow cytometry quantifications of tubulin were carried out. Quantification of tubulin by Western blotting (Fig. 1C), using GAPDH as a loading control, showed that the total amounts of tubulin (either polymerized or not) were similar in infected and uninfected cells. To assess the amount of polymerized tubulin, we extracted soluble proteins from the cytoplasm by permeabilizing the cells during the fixation step of flow cytometry. Under this condition, tubulin staining markedly decreased in infected cells compared to uninfected cells (the ratio of tubulin average intensities of infected versus uninfected cells was 0.59 ± 0.04) (Fig. 1D). These analyses confirm that rotavirus infection induces MT depolymerization and thus disorganizes the MT network without reducing the total amount of tubulin in the cell.

Viroplasms colocalize with tubulin granules and are close to MTs. Rotavirus infection leads to the formation of viral inclusions and damages the MT network. Therefore, we wondered whether these two phenomena could be related. At high magnification, confocal microscopy on rotavirus-infected cells revealed viroplasms (Fig. 2A, NSP2) and the presence of round structures made of tubulin (Fig. 2A, α-tubulin, white arrows). These structures that we termed "tubulin granules" colocalized with viroplasms (Fig. 2A, merged). Viroplasms also seemed to be located in the vicinity of MTs (Fig. 2A, merged). These two observations were confirmed by the analysis of fluorescence intensity profiles of the fluorophores along different lines crossing MTs; representative profiles are presented in Fig. 2B. In areas devoid of viroplasm (along the blue line in Fig. 2A), the MT section is characterized by a rather symmetrical intensity curve (green channel) (Fig. 2B, left panel). We observed, in the presence of a viroplasm (along the red line in Fig. 2A), two peaks for the green channel (Fig. 2B, right panel). The higher peak corresponds to a MT and the smaller one to a tubulin granule. The curve of the red channel corresponds to NSP2 and thus to a viroplasm. The relative position of the two profiles demonstrates that the viroplasm colocalizes with a tubulin granule and the immunostaining of the viroplasm overlaps the immunostaining of the MT. These observations suggest that tubulin is present inside the viroplasms and that viroplasms could be bound to MTs.

MTs are not required for viroplasm formation. Since viroplasms seem bound to MTs, we investigated the requirement of MTs in viroplasm formation. We therefore depolymerized MTs with nocodazole before, during, and after rotavirus infection. As shown in Fig. S2A in the supplemental material, mock-infected and nocodazole-treated cells lost almost all their MTs after a 2-h nocodazole treatment and their centrosomes are intensely stained (white arrows, Fig. S2A in the supplemental material). We also noticed in their cytoplasms the presence of small tubulin granules. Figure 2C shows epifluorescence microscopy images of rotavirus-infected cells treated with nocodazole from 1 h before infection to 6 h postinfection. A 2-h nocodazole treatment ensured that the microtubule network did not exist anymore at the time of virus adsorption, and treatment was maintained during infection to avoid the rebuilding of the network. Despite the absence of an intact MT network, viroplasm formation was not altered. Rotavirus production was also not affected when the infection was performed in the presence of nocodazole (data not shown). The MT network is thus not essential for viroplasm formation or for the viral cycle. These images also show the absence of viroplasm at the centrosome (white arrows, Fig. 2C, merged). The colocalization between viroplasms and the tubulin granules, as suggested in Fig. 2C, was confirmed by confocal microscopy (see Fig. S2B in the supplemental material). This colocalization of tubulin granules with viroplasms suggests once again the presence of tubulin in viroplasms, as previously proposed (Fig. 2A).

Whenever nocodazole was added (before or after rotavirus infection), viroplasm distribution in the cytoplasm was not altered (Fig. S2C in the supplemental material shows cells treated with nocodazole 4 h postinfection). These data suggest that the MT network has no impact on the location of viroplasms.

Tubulin directly interacts *in vitro* with NSP2 but not with NSP5. NSP2 and NSP5 are essential for viroplasm formation. Therefore, we investigated whether NSP2 or NSP5 could directly interact with tubulin *in vitro* by affinity chromatography with purified proteins. Recombinant NSP2 was purified to homogeneity under native conditions (Fig. 3A, lane 1) and covalently cross-linked to activated Sepharose beads. Highly pure tubulin dimers, as analyzed by size exclusion chromatography (data not shown) and shown in Fig. 3A, lane 6, were retained by NSP2-coupled beads (Fig. 3A, lane 4) but not by uncoupled Sepharose beads used as a negative control (Fig. 3A, lane 2), showing that the interaction between NSP2 and tubulin is direct.

NSP5 S2A interaction with tubulin was tested with the same strategy. Purified untagged recombinant NSP5 S2A (Fig. 3B, lane 1) was cross-linked to activated Sepharose beads and incubated with either tubulin or NSP2. Under the same conditions that allowed NSP2-tubulin interaction, NSP5 S2A did not interact with tubulin (Fig. 3B, lane 2) but interacted with NSP2 (data not shown). The latter result points out that the absence of interaction between NSP5 S2A and tubulin is not due to misfolded NSP5 S2A.

The positively charged grooves of NSP2 are the primary binding sites of tubulin. To identify the region of NSP2 involved in tubulin binding, we imaged NSP2 alone and in complex with tubulin by electron microscopy (EM). NSP2 prepa-

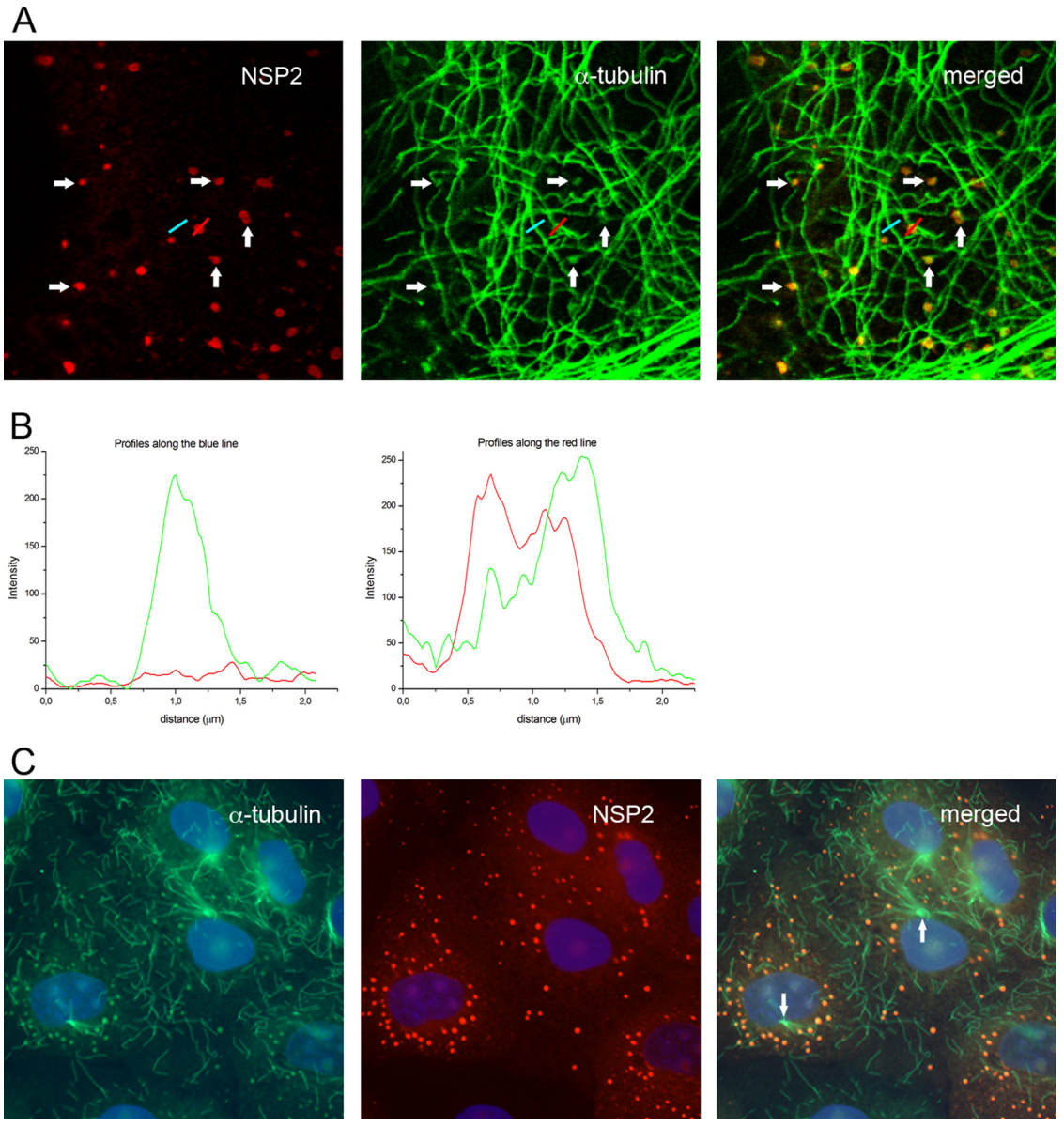

FIG. 2. Viroplasms colocalize with tubulin granules and are close to MTs. (A) MA104 cells were infected by rotavirus strain RF at an MOI of 5 and then fixed at 6 h postinfection with PFA. Cells were immunostained with rabbit anti-NSP2 pAb and then with Alexa Fluor 546-conjugated goat anti-rabbit IgG (red) together with FITC-conjugated mouse anti-α-tubulin MAb (green). Cells were imaged using a confocal microscope in a sequential mode. Note: given the low fluorescence of the remaining MTs in the viroplasm area (Fig. 1B), the 488-nm laser power and photomultiplier gain of the confocal microscope had to be increased to image MTs near viroplasms in this area. This results in the saturation of the signals of some MTs (bottom right corner of the first panel in Fig. 2A), and the image might thus look different from Fig. 1B. Arrows point at some remarkable regions discussed in the text. (B) The fluorescence intensity of the probes along colored lines indicated in panel A was plotted. The green curve is for the green channel (tubulin), and the red curve is for the red channel (NSP2). (C) MA104 cells were treated as described previously except that 2 μM nocodazole was added to the medium at 1 h before infection. Cells were imaged with an epifluorescence microscope.

rations were very homogenous (Fig. 4A, upper left panels). The images show different views, in particular some exhibiting 4-fold symmetry (top views of lower left panel, Fig. 4A) and others exhibiting 2-fold symmetry (side views of lower left panel, Fig. 4A), suggesting the existence of 4- and 2-fold symmetry axes. Multistatistical analysis (45) of the data sets showed two eigenimages exhibiting 4- and 2-fold symmetry (data not shown), similar to the averages of some classes thus defined (enlarged images labeled "mean," Fig. 4A). Imposing the symmetry on the average images (enlarged images labeled "computed," Fig. 4A) did not change greatly the averages, showing that the 4- and 2-fold symmetry axes were independent. Analyses of the particles were thus done using D4 symmetry. The reconstruction of NSP2 from the rotavirus RF strain (Fig. 4A, second panel) has a doughnut-shaped structure with a 35-Å central hole and prominent grooves, as expected from the crystallo-

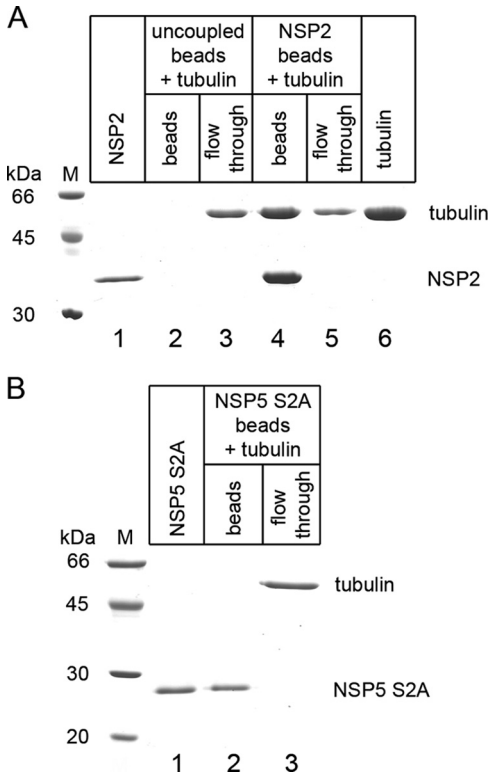

FIG. 3. Tubulin directly interacts *in vitro* with NSP2 but not with NSP5 S2A. (A) Purified NSP2 (lane 1) and tubulin (lane 6) were analyzed by SDS-PAGE and Coomassie blue staining. Either uncoupled Sepharose beads or NSP2-cross-linked Sepharose beads were incubated with tubulin. Flowthroughs and beads were analyzed by SDS-PAGE and Coomassie blue staining. Flowthroughs were loaded on lane 3 (uncoupled Sepharose beads) and lane 5 (NSP2-cross-linked Sepharose beads). Beads were loaded on lane 2 (uncoupled Sepharose beads) and lane 4 (NSP2-cross-linked Sepharose beads). The presence of NSP2 in lane 4 corresponds to the release of NSP2 subunits uncoupled with the Sepharose matrix. (B) Purified NSP5 S2A (lane 1) was analyzed by SDS-PAGE and Coomassie blue staining. NSP5 S2A-cross-linked Sepharose beads were incubated with tubulin. The flowthrough and beads were analyzed by SDS-PAGE and Coomassie blue staining. The flowthrough was loaded on lane 3, and the beads were loaded on lane 2.

graphic structure of NSP2 from the rotavirus SA11 strain (21). The SA11 NSP2 X-ray structure fits well in our reconstruction, without significant alterations (Fig. 4A, third panel). At this low resolution, the structures of RF NSP2 and SA11 NSP2 are identical.

By electron microscopy, the NSP2-tubulin complex also appeared as a doughnut-shaped structure with a much broader polymorphism (Fig. 4B, first and second panels). This polymorphism and the associated difficulty of selecting particles in low-contrast images prevented us from carrying out cryo-EM observations; we therefore used negative-staining electron microscopy despite its low-resolution results. We interpret this polymorphism as a consequence of a variable stoichiometry of NSP2-tubulin complexes and different binding geometries between NSP2 and tubulin. EM reconstruction of the tubulin-NSP2 complex was performed using RF NSP2 reconstruction as the initial reference model. Owing to this polymorphism and to negative-staining electron microscopy limitations, adding more images to perform our reconstruction would not have allowed us to reach a much better resolution. The difference between the complex reconstruction and the NSP2 reconstruction pointed out different regions of extra electron densities (colored in green in Fig. 4B, third panel) that we attributed to tubulin. These extra electron densities are located above the 35-Å central hole and mostly in the grooves at one of the 2-fold axes. Tubulin is a heterodimer made of one α subunit and one β subunit. The extra density in NSP2 grooves that we attributed to tubulin cannot embed either the structure of a tubulin dimer or that of one of the tubulin subunits. This result demontrates a great variability of contacts of tubulin in the grooves of NSP2. A precise fit between the reconstruction and the atomic models is thus difficult to perform. When one of the two subunits of a tubulin heterodimer was fitted in the extra density present in the groove, the orientation that minimized clashes between protein chains was obtained when the C-terminal H12 α-helix of this tubulin subunit occupied the electron density seen in the EM reconstruction (Fig. 4C). Interestingly, these grooves are highly positively charged (21) and the H12 helix is acidic.

Because NSP5 also binds to these grooves of NSP2 (22), we tested whether NSP5 and tubulin could compete for NSP2 binding. We thus incubated tubulin with NSP2-coupled beads prior to the addition of NSP5 (see Fig. S3A in the supplemental material). Alternatively, NSP5 was incubated with NSP2-coupled beads before tubulin was added (see Fig. S3B in the supplemental material). The amounts of NSP5 and tubulin bound to NSP2-coupled beads were analyzed on Coomassie blue-stained SDS-PAGE gels. When tubulin was added before NSP5, tubulin inhibited NSP5 binding to NSP2 (compare lanes 3 in Fig. S3A and B in the supplemental material). When tubulin was added after NSP5, tubulin dissociated NSP2-NSP5 complexes (compare Fig. S3B, lanes 1 and 3). Hence, tubulin and NSP5 compete to bind to NSP2.

Because RNA also binds to these grooves of NSP2 (22), we tested whether RNA and tubulin could also compete for NSP2 binding to further confirm that the positively charged grooves of NSP2 are tubulin binding sites. RNA binding to NSP2 was first verified by an electrophoretic mobility shift assay (see Fig. S4 in the supplemental material). We then incubated NSP2 with tubulin-coupled beads prior to the addition of RNA. Alternatively, NSP2 was incubated with RNA and then tubulin-coupled beads were added. After several washes, the amount of NSP2 bound to tubulin-coupled beads was quantified by densitometry on Coomassie blue-stained SDS-PAGE gels. Whenever RNA was added, after tubulin (Fig. 4D, black bars) or prior to tubulin (Fig. 4D, gray bars), it competed with tubulin to bind to NSP2. Thus, binding sites of RNA and tubulin on NSP2 octamers overlap.

Lysines 37, 38, 58, and 59 and arginines 60 and 68 are in NSP2 grooves, and their simultaneous mutation into glutamine decreases RNA binding without modifying the overall folding of NSP2 (46). To further confirm the tubulin binding site on NSP2, we tested whether NSP2 K37Q K38Q K58Q K59Q R60Q R68Q could bind to tubulin-coupled beads. The mutation of these six residues on NSP2 decreased the amount of NSP2 bound to tubulin by 80% (Fig. 4E). These residues must thus be important for the interaction of NSP2 with tubulin. All

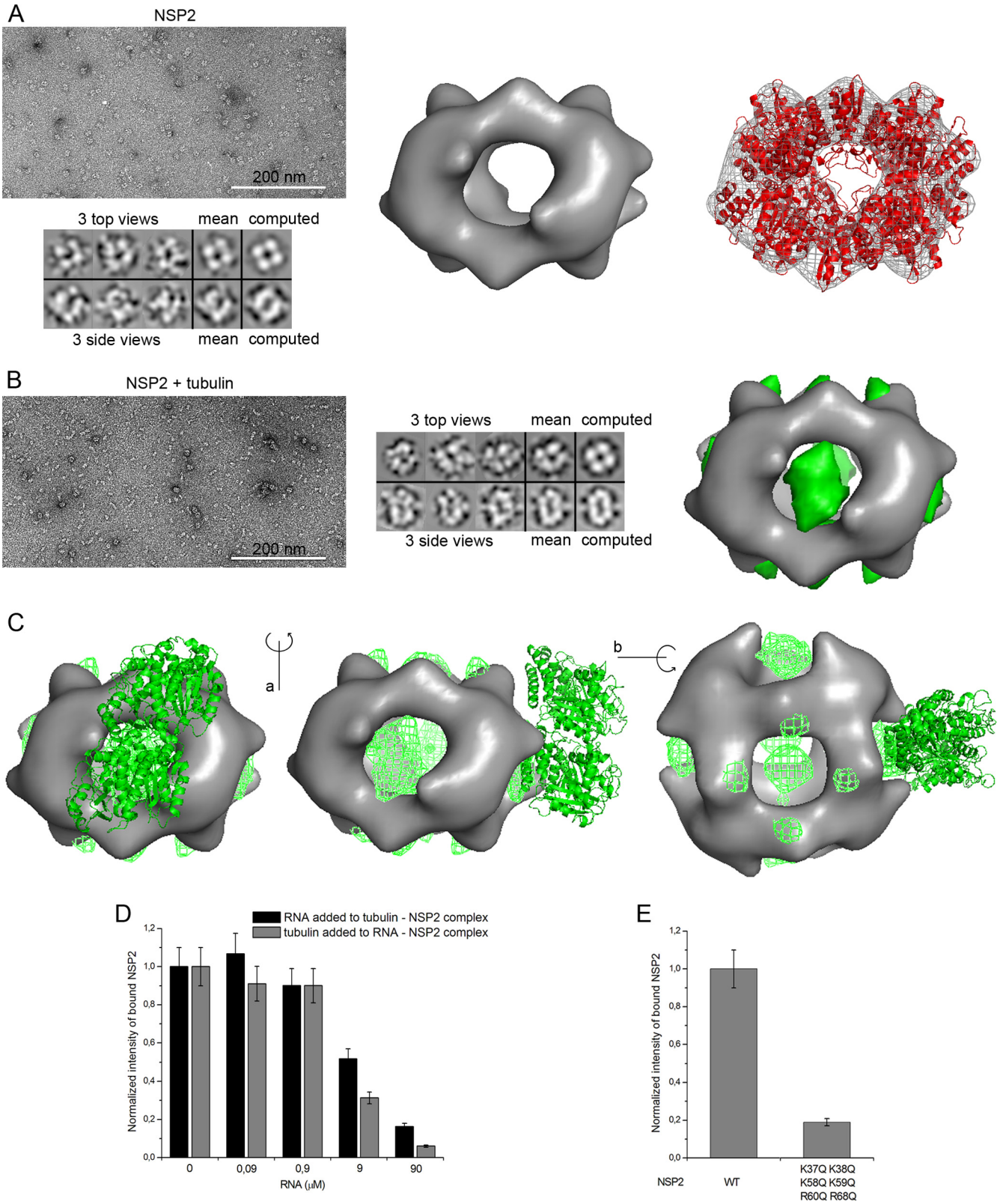

FIG. 4. Tubulin binds to NSP2 through the positively charged grooves of NSP2. (A) NSP2 alone (upper left panel) was visualized by negative-staining electron microscopy. Lower left panel presents six larger images with different views: three labeled "top views" exhibiting 4-fold symmetry and three labeled "side views" exhibiting 2-fold symmetry. The images labeled "mean" correspond to the average of the three views. The images labeled "computed" were generated by imposing the appropriate symmetry on the "mean" images. The second panel shows a three-dimensional (3-D) reconstruction of NSP2 alone. The structure of NSP2 from the SA11 strain was fitted in our EM reconstruction (third panel).

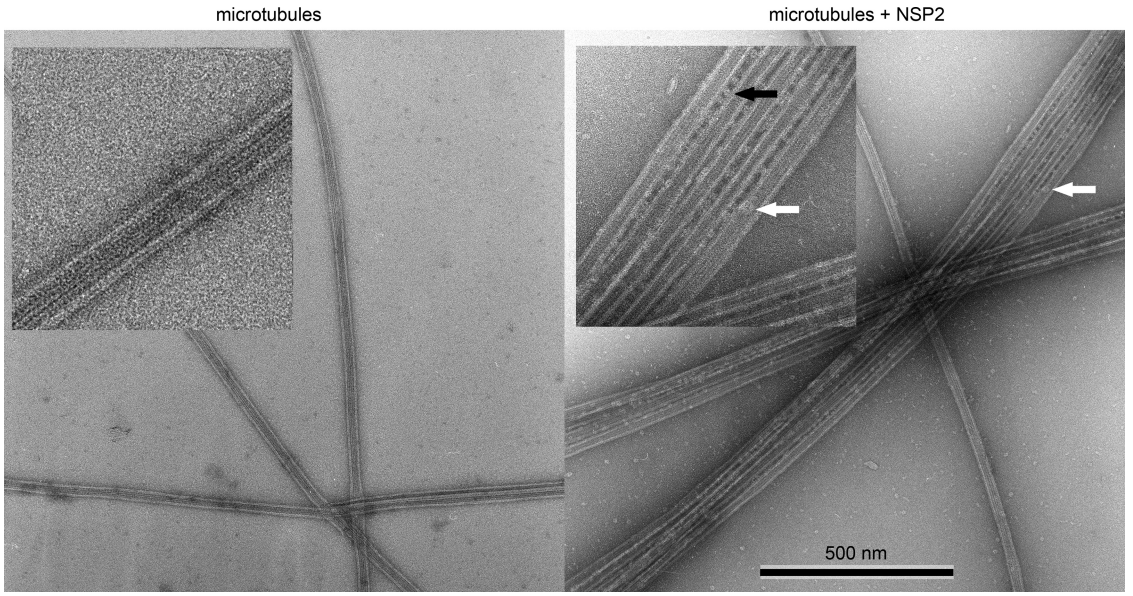

FIG. 5. NSP2 binds and aggregates stabilized MTs. Paclitaxel-stabilized MTs incubated without (left panel) or with (right panel) 0.05 μM NSP2 were imaged by electron microscopy. The white arrow points at a molecule of NSP2 bound to a single MT, whereas the black arrow points at a molecule of NSP2 linking two MTs.

these experiments highlight that tubulin binds to the grooves of NSP2.

***In vitro*, NSP2 binds and aggregates stabilized MTs.** Tubulin is the building block of MTs; tubulin dimers assemble to form protofilaments, and MTs are made of laterally associated protofilaments. Therefore, we investigated the binding of NSP2 to paclitaxel-stabilized MTs by electron microscopy using negative staining. In the absence of NSP2, stabilized MTs appeared as single straight tubes (Fig. 5, left panel). When stabilized MTs were incubated with 0.05 μM NSP2, NSP2 appeared as doughnut-shaped particles on stabilized MTs (white arrows, Fig. 5, right panel), showing that some NSP2 octamers were bound to stabilized MTs. However, these MTs were neither uniformly nor periodically decorated by NSP2. Moreover, only few NSP2 octamers were bound to stabilized MTs. This observation suggests a rather weak interaction between NSP2 and stabilized MTs. NSP2 also induced the formation of MT aggregates, illustrated by NSP2 linking two stabilized MTs (black arrow, Fig. 5, right panel).

NSP2 colocalizes with tubulin and damages MTs *in vivo*. Since NSP2 directly interacts with tubulin *in vitro*, we investigated the effects of its expression on MTs *in vivo* in the absence of rotavirus infection. NSP2 is difficult to express with an expression system based on nuclear polymerase II transcription (our unpublished results). We therefore expressed NSP2 under the control of the T7 RNA polymerase promoter in BSR-T7/5 cells that constitutively express cytoplasmic T7 RNA polymerase (7). This expression system circumvents the nuclear transcription problem and avoids MT damages induced by vaccinia virus infection (34). When expressed alone, NSP2 drastically remodeled the MT network (Fig. 6, panel B compared to panel A). Compared to those in mock-transfected cells (Fig. 6A), MTs were fragmented and shorter in NSP2-expressing cells (Fig. 6B), forming a loose network. We also noticed numerous NSP2 foci and the presence of faintly stained tubulin dots, which colocalized with NSP2 foci (white arrows, Fig. 6B). Moreover, the coexpression of NSP5 S2A with NSP2 considerably changed the localization of NSP2 and drastically reduced the number of tubulin granules (Fig. 6C). The presence of NSP5 with NSP2 induced the formation of VLS (white arrows, Fig. 6C). Tubulin clearly colocalized with VLS (Fig. 6C), a result similar to the colocalization of tubulin with viroplasms during rotavirus infection. These effects of NSP2 ex-

(B) NSP2 in complex with tubulin (ratio, 1 octamer of NSP2 with 4 dimers of tubulin) (first panel) was visualized by negative-staining electron microscopy. The second panel presents six larger images with different views: three labeled "top views" exhibiting 4-fold symmetry and three labeled "side views" exhibiting 2-fold symmetry. The images labeled "mean" correspond to the average of the three views. The images labeled "computed" were generated by imposing the appropriate symmetry on the "mean" images. The third panel shows a 3-D reconstruction of NSP2 in complex with tubulin; densities in green correspond to extra densities compared to NSP2 alone. (C) Model of the interaction between NSP2 and tubulin. The second view corresponds to a 90° rotation of the first view along axis a, and the third view corresponds to a 90° rotation of the second view along axis b. (D) Tubulin-cross-linked Sepharose beads were incubated with wild-type (wt) NSP2 before (black bars) or after (gray bars) the addition of different concentrations of RNA. Beads were analyzed by SDS-PAGE and Coomassie blue staining and quantified by densitometry. Intensity was normalized to 1 in the absence of RNA. (E) Tubulin-cross-linked Sepharose beads were incubated with wt NSP2 or NSP2 K37Q K38Q K58Q K59Q R60Q R68Q. Beads were analyzed by SDS-PAGE and Coomassie blue staining and quantified by densitometry. Intensity was normalized to 1 for wt NSP2.

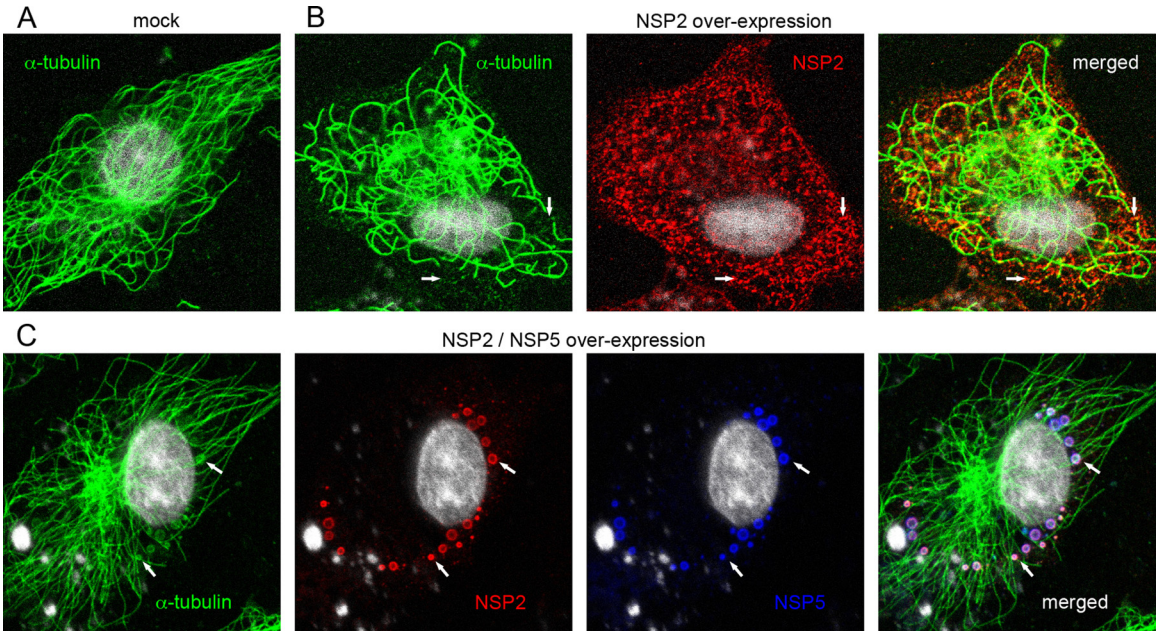

FIG. 6. Expression of NSP2 without or with NSP5 S2A in BSR-T7/5 cells. (A, B, and C) BSR-T7/5 cells were either mock transfected (A), or transfected with NSP2 (B), or NSP2 and NSP5 S2A (C) expression vectors. At 24 h posttranfection, cells were lysed during 2 min with 0.5% Triton X-100 prior to PFA fixation. Cells were immunostained with rabbit anti-NSP2 pAb together with mouse anti-NSP5 MAb (α-NSP5), then with Alexa Fluor 546-conjugated goat anti-rabbit IgG (red) together with Alexa Fluor 633-conjugated goat anti-mouse IgG (blue), and then with FITC-conjugated mouse anti-α-tubulin MAb (green). The nuclei were stained with DAPI (gray). Cells were imaged using a confocal microscope in a sequential mode. Arrows point at some remarkable regions discussed in the text.

pression on the MT network are strongly reminiscent of those previously observed for rotavirus-infected cells (Fig. 1 and 2).

DISCUSSION

In this study, we highlight rotavirus NSP2 as the main factor for MT reorganization observed during viral infection. The regions of NSP2 involved in the direct interaction with tubulin are identified, and we decipher the depolymerizing effects of this interaction on MTs. Our biochemical studies allow us to investigate the mechanism by which NSP2 depolymerizes MTs *in vivo*. Based on these data, we propose that a similar mechanism takes place in the cell during rotavirus infection.

Using an affinity chromatography assay with purified proteins, we showed that NSP2 and dimeric tubulin directly interact. In the same conditions, NSP5 interacts with NSP2 but not with tubulin. By coimmunoprecipitation, a tubulin-NSP5 interaction has been previously proposed (9) that indeed could result from an indirect interaction between NSP5 and tubulin through an unidentified cellular or viral protein (most probably NSP2). The use of a T7 recombinant vaccinia virus to express NSP5 (9) might also have somehow promoted an interaction between NSP5 and tubulin, as vaccinia virus is known to damage the MT network (34). The involvement of phosphorylated forms of NSP5 in the recognition of tubulin (which we would not have detected with protein produced in bacteria) is very unlikely because adding negative charges on NSP5 should rather prevent its interaction with acidic proteins like tubulin.

Our biochemical experiments demonstrated that the interaction between NSP2 and dimeric tubulin is direct. The positively charged grooves of NSP2 are identified as the primary binding sites for tubulin, by EM reconstruction, RNA competition assays, and site-directed mutagenesis. Comparison of electron densities between NSP2 alone and NSP2 in complex with tubulin reveals extra electron densities in the deep grooves of NSP2 octamers. These densities can only accommodate a part of the X-ray structure of a tubulin monomer, revealing a great structural variability that intrinsically limits the resolution of our study. The contact variability confirms the poor binding specificity of this NSP2 region as previously reported (22, 44). The fitting of the tubulin X-ray model into the EM reconstruction suggests that the C-terminal H12 α-helix of tubulin is likely to be involved in NSP2 binding. Indeed, the tubulin H12 helix is negatively charged and NSP2 grooves are lined by positively charged residues. Moreover, the crystallographic structures of the two proteins reveal that in this orientation, dimeric tubulin has access to NSP2 grooves without any major steric hindrance. The involvement of tubulin helix H12 in the contacts with NSP2 is also reinforced by the binding of NSP2 to polymerized tubulin, as visualized by EM, because this helix is indeed present on the outer surface of MTs (50).

Electron microscopy showed that NSP2 binds to stabilized MTs and aggregates MTs. However, EM also revealed that the majority of NSP2 octamers were not bound to MTs, suggesting a poor binding affinity of NSP2 to MTs. This assumption is reinforced by the absence of an obvious colocalization of NSP2 with MTs in NSP2-expressing cells. When NSP2 was overexpressed, MTs were fragmented and the MT network was damaged, showing that NSP2 induces MT depolymerization. Several mechanisms can explain the depolymerization process of MTs induced by NSP2. First, tubulin polymerizes into MTs in

the presence of GTP and MTs depolymerize in the presence of GDP. Since NSP2 has a NTPase activity, it could make MTs shrink by decreasing GTP concentration and increasing GDP concentration. However, this mechanism is not predominant because we showed that a NSP2 mutant deficient in NTPase activity (NSP2 H225A) (11) could still bind to tubulin *in vitro* and drastically damage MTs *in vivo* (see Fig. S5 in the supplemental material). Second, MTs are in equilibrium with free tubulin, whose concentration *in vitro* equals its critical concentration. Thus, binding of NSP2 to dimeric tubulin lowers the concentration of free tubulin and, as a consequence, MTs depolymerize until the free tubulin concentration reaches its critical concentration. We cannot exclude an additional direct damaging effect of NSP2 upon MT binding.

In this report, we also showed that early in infection, rotavirus strain RF does not modify the amount of tubulin per cell but induces the depolymerization of MTs. The MT network is highly disturbed, less dense, more present at the cell periphery, and not well organized from the centrosome, which becomes hardly visible. We also notice the presence of tubulin granules that colocalize with viroplasms. These findings differ with previously published results with rhesus rotavirus (47). Weclewicz et al. did not notice any MT network change during the 16 h that followed RRV infection in CV1 cells (47); however, the amount of tubulin in the cytoplasm (free and incorporated in MTs) was not quantified. Moreover, some tubulin granules, visible in their study, were overlooked. The extent of the MT modifications induced by rotavirus could depend on variations of the stability of the MT network between cell lines or on the cell physiological state, as suggested by differences observed between differentiated and undifferentiated Caco-2 cells (6).

Our data indicate that NSP2 damages the MT network by inducing MT depolymerization and that NSP2 directly interacts with tubulin dimers. Moreover, we show that tubulin granules colocalize with viroplasms and VLS, strongly suggesting that tubulin is a viroplasm component. For these reasons, we propose that the reorganizations and perturbations of the MT network occurring during the rotavirus infection are mostly due to NSP2. By holding tubulin inside viroplasms, NSP2 induces a decrease in tubulin concentration in the cytoplasm that affects MT dynamics and stability, as observed in NSP2-overexpressing cells. Damages to the MT network are less important in infected cells (Fig. 1B) or in cells coexpressing NSP2 and NPS5 (Fig. 6C) than in NSP2-expressing cells (Fig. 6B). Since we were also able to perform competitions between NSP5, tubulin, and RNA for their binding to NSP2 (Fig. 4; see Fig. S3 in the supplemental material), the effect of NSP2 on MTs *in vivo* is thus tuned by NSP5 and/or viral RNA, which also bind to the positively charged grooves of NSP2. *In vivo*, the phosphorylation state of NSP5 (1, 36, 48), by adding negative charges to the protein, may also play a role in the regulation of these competitions.

Experiments with nocodazole also allowed us to show that viroplasms colocalize with tubulin granules, similar to secondary microtubule organizing centers (MTOCs) observed in different cell lines treated with nocodazole (5, 8, 13, 25). We thus propose that viroplasms preferentially form at secondary MTOCs during rotavirus infection.

The role of the alteration of the MT network during rotavirus infection remains an intriguing question. Indeed, cell treatment with an MT-depolymerizing drug does not prevent the formation of viroplasms (Fig. 2) (9), but the growth and fusion of viroplasms, observed by Eichwald et al. (16) later in infection, are inhibited by nocodazole (9). Similar results were also reported for orthoreovirus, another member of the *Reoviridae* family (12, 15). Moreover, as the viral titer of rotavirus was not significantly altered by the presence of nocodazole during the entire infection (our unpublished results), the MT network is not essential for the viral cycle. However, to perform its viral cycle, rotavirus hijacks cell machineries and inhibits such cell functions as cellular protein synthesis (33) or interferon expression (2). MT damaging is another means to shut off cell functions and signal pathways which can also be involved in cell response to viral infection. For instance, autophagy and proteasome degradation involve protein trafficking along MTs to the aggresome, located near the centrosome (for a review, see reference 49). Thus, disturbing the MTs and the centrosome could prevent the cell from addressing viral proteins and viroplasms to the aggresome for degradation. Moreover, anchoring viroplasms on MTs, as suggested by viroplasms located close to MTs, may further inhibit viroplasm transport by molecular motors.

In summary, our results show that NSP2 directly binds to tubulin through its positively charged grooves and that NSP2 induces the collapse of the MT network *in vivo*. We also highlight that rotavirus infection induces a rearrangement in the MT network, which we can mostly assign to NSP2. We also suggest that NSP2 is involved in viroplasm nucleation at particular tubulin granules and sequesters tubulin inside viroplasms, inducing MT depolymerization and thus inhibiting cellular trafficking and functions. The sequestration of a major cellular building block affects its polymerization dynamics, which probably leads to a complete deregulation of the cellular machinery. This mechanism illustrates once again how viruses develop strategies to detour cellular mechanisms for their own benefit.

ACKNOWLEDGMENTS

We thank S. Bölte and M. N. Soler for expert support with confocal microscopy and analyses and M. Bourge and S. Brown for flow cytometry experiments. We also thank A. Guillot from the PAPSS laboratory (INRA, Jouy en Josas, France) for his help in mass spectrometry identification of the recombinant proteins; A. Charpilienne, who produced and determined the titer of the rotavirus RF strain; and C. Laroche for some plasmid constructions. We are grateful to D. Blondel, Y. Gaudin, M. Knossow, and J. Menetrey for helpful discussions.

D.M. designed the research and performed experiments; M.D. purified the anti-NSP2 pAb; J.L. performed electron microscopy observations and reconstructions; D.M. and J.L. analyzed the data; D.M., J.L., and D.P. wrote the paper.

This work has been supported by a grant from Département Santé Animale, INRA, France, and has benefited from the facilities and expertise of the IMAGIF Cell Biology Unit of the Gif campus (www.imagif.cnrs.fr) supported by the Conseil Général de l'Essonne.

REFERENCES

1. **Afrikanova, I., M. C. Miozzo, S. Giambiagi, and O. Burrone.** 1996. Phosphorylation generates different forms of rotavirus NSP5. J. Gen. Virol. **77**(part 9)**:**2059–2065.
2. **Barro, M., and J. T. Patton.** 2007. Rotavirus NSP1 inhibits expression of type I interferon by antagonizing the function of interferon regulatory factors IRF3, IRF5, and IRF7. J. Virol. **81:**4473–4481.
3. **Been, M. D.** 2006. HDV ribozymes. Curr. Top. Microbiol. Immunol. **307:** 47–65.
4. **Berkova, Z., S. E. Crawford, G. Trugnan, T. Yoshimori, A. P. Morris, and**

M. K. Estes. 2006. Rotavirus NSP4 induces a novel vesicular compartment regulated by calcium and associated with viroplasms. J. Virol. **80:**6061–6071.
5. **Bre, M. H., T. E. Kreis, and E. Karsenti.** 1987. Control of microtubule nucleation and stability in Madin-Darby canine kidney cells: the occurrence of noncentrosomal, stable detyrosinated microtubules. J. Cell Biol. **105:** 1283–1296.
6. **Brunet, J. P., N. Jourdan, J. Cotte-Laffitte, C. Linxe, M. Geniteau-Legendre, A. Servin, and A. M. Quero.** 2000. Rotavirus infection induces cytoskeleton disorganization in human intestinal epithelial cells: implication of an increase in intracellular calcium concentration. J. Virol. **74:**10801–10806.
7. **Buchholz, U. J., S. Finke, and K. K. Conzelmann.** 1999. Generation of bovine respiratory syncytial virus (BRSV) from cDNA: BRSV NS2 is not essential for virus replication in tissue culture, and the human RSV leader region acts as a functional BRSV genome promoter. J. Virol. **73:**251–259.
8. **Bulinski, J. C., J. E. Richards, and G. Piperno.** 1988. Posttranslational modifications of alpha tubulin: detyrosination and acetylation differentiate populations of interphase microtubules in cultured cells. J. Cell Biol. **106:** 1213–1220.
9. **Cabral-Romero, C., and L. Padilla-Noriega.** 2006. Association of rotavirus viroplasms with microtubules through NSP2 and NSP5. Mem. Inst. Oswaldo Cruz **101:**603–611.
10. **Campagna, M., C. Eichwald, F. Vascotto, and O. R. Burrone.** 2005. RNA interference of rotavirus segment 11 mRNA reveals the essential role of NSP5 in the virus replicative cycle. J. Gen. Virol. **86:**1481–1487.
11. **Carpio, R. V., F. D. Gonzalez-Nilo, H. Jayaram, E. Spencer, B. V. Prasad, J. T. Patton, and Z. F. Taraporewala.** 2004. Role of the histidine triad-like motif in nucleotide hydrolysis by the rotavirus RNA-packaging protein NSP2. J. Biol. Chem. **279:**10624–10633.
12. **Carvalho, J., M. M. Arnold, and M. L. Nibert.** 2007. Silencing and complementation of reovirus core protein mu2: functional correlations with mu2-microtubule association and differences between virus- and plasmid-derived mu2. Virology **364:**301–316.
13. **Chabin-Brion, K., J. Marceiller, F. Perez, C. Settegrana, A. Drechou, G. Durand, and C. Pous.** 2001. The Golgi complex is a microtubule-organizing organelle. Mol. Biol. Cell **12:**2047–2060.
14. **Conway, J. F., and A. C. Steven.** 1999. Methods for reconstructing density maps of "single" particles from cryoelectron micrographs to subnanometer resolution. J. Struct. Biol. **128:**106–118.
15. **Dales, S.** 1963. Association between the spindle apparatus and reovirus. Proc. Natl. Acad. Sci. U. S. A. **50:**268–275.
16. **Eichwald, C., J. F. Rodriguez, and O. R. Burrone.** 2004. Characterization of rotavirus NSP2/NSP5 interactions and the dynamics of viroplasm formation. J. Gen. Virol. **85:**625–634.
17. **Elroy-Stein, O., and B. Moss.** 1990. Cytoplasmic expression system based on constitutive synthesis of bacteriophage T7 RNA polymerase in mammalian cells. Proc. Natl. Acad. Sci. U. S. A. **87:**6743–6747.
18. **Fabbretti, E., I. Afrikanova, F. Vascotto, and O. R. Burrone.** 1999. Two non-structural rotavirus proteins, NSP2 and NSP5, form viroplasm-like structures in vivo. J. Gen. Virol. **80**(part 2)**:**333–339.
19. **Gardet, A., M. Breton, P. Fontanges, G. Trugnan, and S. Chwetzoff.** 2006. Rotavirus spike protein VP4 binds to and remodels actin bundles of the epithelial brush border into actin bodies. J. Virol. **80:**3947–3956.
20. **Harb, M., M. M. Becker, D. Vitour, C. H. Baron, P. Vende, S. C. Brown, S. Bolte, S. T. Arold, and D. Poncet.** 2008. Nuclear localization of cytoplasmic poly(A)-binding protein upon rotavirus infection involves the interaction of NSP3 with eIF4G and RoXaN. J. Virol. **82:**11283–11293.
21. **Jayaram, H., Z. Taraporewala, J. T. Patton, and B. V. Prasad.** 2002. Rotavirus protein involved in genome replication and packaging exhibits a HIT-like fold. Nature **417:**311–315.
22. **Jiang, X., H. Jayaram, M. Kumar, S. J. Ludtke, M. K. Estes, and B. V. Prasad.** 2006. Cryoelectron microscopy structures of rotavirus NSP2-NSP5 and NSP2-RNA complexes: implications for genome replication. J. Virol. **80:**10829–10835.
23. **Kumar, M., H. Jayaram, R. Vasquez-Del Carpio, X. Jiang, Z. F. Taraporewala, R. H. Jacobson, J. T. Patton, and B. V. Prasad.** 2007. Crystallographic and biochemical analysis of rotavirus NSP2 with nucleotides reveals a nucleoside diphosphate kinase-like activity. J. Virol. **81:**12272–12284.
24. **Lopez, T., M. Rojas, C. Ayala-Breton, S. Lopez, and C. F. Arias.** 2005. Reduced expression of the rotavirus NSP5 gene has a pleiotropic effect on virus replication. J. Gen. Virol. **86:**1609–1617.
25. **Luders, J., and T. Stearns.** 2007. Microtubule-organizing centres: a re-evaluation. Nat. Rev. Mol. Cell Biol. **8:**161–167.
26. **Ludtke, S. J., P. R. Baldwin, and W. Chiu.** 1999. EMAN: semiautomated software for high-resolution single-particle reconstructions. J. Struct. Biol. **128:**82–97.
27. **Moss, B., and B. M. Ward.** 2001. High-speed mass transit for poxviruses on microtubules. Nat. Cell Biol. **3:**E245–E246.
28. **Navaza, J.** 2003. On the three-dimensional reconstruction of icosahedral particles. J. Struct. Biol. **144:**13–23.
29. **Nejmeddine, M., G. Trugnan, C. Sapin, E. Kohli, L. Svensson, S. Lopez, and J. Cohen.** 2000. Rotavirus spike protein VP4 is present at the plasma membrane and is associated with microtubules in infected cells. J. Virol. **74:**3313–3320.
30. **Netherton, C., K. Moffat, E. Brooks, and T. Wileman.** 2007. A guide to viral inclusions, membrane rearrangements, factories, and viroplasm produced during virus replication. Adv. Virus Res. **70:**101–182.
31. **Parashar, U. D., C. J. Gibson, J. S. Bresse, and R. I. Glass.** 2006. Rotavirus and severe childhood diarrhea. Emerg. Infect. Dis. **12:**304–306.
32. **Parker, J. S., T. J. Broering, J. Kim, D. E. Higgins, and M. L. Nibert.** 2002. Reovirus core protein mu2 determines the filamentous morphology of viral inclusion bodies by interacting with and stabilizing microtubules. J. Virol. **76:**4483–4496.
33. **Piron, M., P. Vende, J. Cohen, and D. Poncet.** 1998. Rotavirus RNA-binding protein NSP3 interacts with eIF4GI and evicts the poly(A) binding protein from eIF4F. EMBO J. **17:**5811–5821.
34. **Ploubidou, A., V. Moreau, K. Ashman, I. Reckmann, C. Gonzalez, and M. Way.** 2000. Vaccinia virus infection disrupts microtubule organization and centrosome function. EMBO J. **19:**3932–3944.
35. **Ploubidou, A., and M. Way.** 2001. Viral transport and the cytoskeleton. Curr. Opin. Cell Biol. **13:**97–105.
36. **Poncet, D., P. Lindenbaum, R. L'Haridon, and J. Cohen.** 1997. In vivo and in vitro phosphorylation of rotavirus NSP5 correlates with its localization in viroplasms. J. Virol. **71:**34–41.
37. **Schuck, P., Z. Taraporewala, P. McPhie, and J. T. Patton.** 2001. Rotavirus nonstructural protein NSP2 self-assembles into octamers that undergo ligand-induced conformational changes. J. Biol. Chem. **276:**9679–9687.
38. **Silvestri, L. S., Z. F. Taraporewala, and J. T. Patton.** 2004. Rotavirus replication: plus-sense templates for double-stranded RNA synthesis are made in viroplasms. J. Virol. **78:**7763–7774.
39. **Smith, G. A., and L. W. Enquist.** 2002. Break ins and break outs: viral interactions with the cytoskeleton of mammalian cells. Annu. Rev. Cell Dev. Biol. **18:**135–161.
40. **Sodeik, B.** 2000. Mechanisms of viral transport in the cytoplasm. Trends Microbiol. **8:**465–472.
41. **Spendlove, R. S., E. H. Lennette, and A. C. John.** 1963. The role of the mitotic apparatus in the intracellular location of reovirus antigen. J. Immunol. **90:**554–560.
42. **Taraporewala, Z., D. Chen, and J. T. Patton.** 1999. Multimers formed by the rotavirus nonstructural protein NSP2 bind to RNA and have nucleoside triphosphatase activity. J. Virol. **73:**9934–9943.
43. **Taraporewala, Z. F., X. Jiang, R. Vasquez-Del Carpio, H. Jayaram, B. V. Prasad, and J. T. Patton.** 2006. Structure-function analysis of rotavirus NSP2 octamer by using a novel complementation system. J. Virol. **80:**7984–7994.
44. **Taraporewala, Z. F., and J. T. Patton.** 2001. Identification and characterization of the helix-destabilizing activity of rotavirus nonstructural protein NSP2. J. Virol. **75:**4519–4527.
45. **van Heel, M., B. Gowen, R. Matadeen, E. V. Orlova, R. Finn, T. Pape, D. Cohen, H. Stark, R. Schmidt, M. Schatz, and A. Patwardhan.** 2000. Single-particle electron cryo-microscopy: towards atomic resolution. Q. Rev. Biophys. **33:**307–369.
46. **Vasquez-Del Carpio, R., F. D. Gonzalez-Nilo, G. Riadi, Z. F. Taraporewala, and J. T. Patton.** 2006. Histidine triad-like motif of the rotavirus NSP2 octamer mediates both RTPase and NTPase activities. J. Mol. Biol. **362:**539–554.
47. **Weclewicz, K., K. Kristensson, and L. Svensson.** 1994. Rotavirus causes selective vimentin reorganization in monkey kidney CV-1 cells. J. Gen. Virol. **75**(part 11)**:**3267–3271.
48. **Welch, S. K., S. E. Crawford, and M. K. Estes.** 1989. Rotavirus SA11 genome segment 11 protein is a nonstructural phosphoprotein. J. Virol. **63:**3974–3982.
49. **Wileman, T.** 2007. Aggresomes and pericentriolar sites of virus assembly: cellular defense or viral design? Annu. Rev. Microbiol. **61:**149–167.
50. **Wolf, S. G., E. Nogales, M. Kikkawa, D. Gratzinger, N. Hirokawa, and K. H. Downing.** 1996. Interpreting a medium-resolution model of tubulin: comparison of zinc-sheet and microtubule structure. J. Mol. Biol. **262:**485–501.
51. **Xu, A., A. R. Bellamy, and J. A. Taylor.** 2000. Immobilization of the early secretory pathway by a virus glycoprotein that binds to microtubules. EMBO J. **19:**6465–6474.